Electronic Supplementary Material (ESI) for Inorganic Chemistry Frontiers.

Supporting Information

Chiral Bis(phthalocyaninato) Terbium Double-decker Compounds with Enhanced Single-Ion Magnet Behavior

Kang Wang, Fang Ma, Dongdong Qi, Xin Chen, Yuxiang Chen, Yan-Cong Chen,

Hao-Ling Sun,* Ming-Liang Tong,* and Jianzhuang Jiang*

Experimental Section

General. *n*-Pentanol was distilled from sodium. Column chromatography was carried out on silica gel (Merck, Kieselgel 60, 70-230 mesh) with the indicated eluents. Tb(acac)$_3$·*n*H$_2$O,[S1] Tb(Pc)(acac),[S2] (R)-/(S)-benzo[b]dinaphtho[2,1-e:1',2'-g][1,4]dioxocine-5,6-dicar-bonitrile,[S3] were prepared according to the published procedures. All other reagents and solvents were used as received.

Electronic absorption spectra were recorded on a Lambda 750 spectrophotometer. IR spectra were recorded as KBr pellets using a Bruker Tensor 37 spectrometer with 2 cm^{-1} resolution. MALDI-TOF mass spectra were taken on a Bruker BIFLEX III ultrahigh-resolution Fourier transformion cyclotron resonance (FT-ICR) mass spectrometer with alpha-cyano-4-hydroxycinnamic acid as matrix. Elemental analyses were performed on an Elementar Vavio El III. CD spectra were recorded using a Jasco J-1500 spectrodichrometer. MCD and magneto-chiral dichroism spectra measurements were made on a JASCO J-1500 spectropolarimeter in the presence of magnetic field (1.6 T) with both parallel and antiparallel fields. For magneto-chiral dichroism spectra measurements, using a reported method,[S4] we measured the absorbance in directions parallel to **H** and then the absorbance in directions antiparallel to **H** in the region of 550-750 nm point-by-point at 0.2 nm. Subsequently, we measured the antiparallel absorbance first and then the parallel absorbance. By repeating this procedure 15-20 times, the data was accumulated, and then the averaged magneto-chiral dichroism spectra were obtained from the difference between the parallel and antiparallel absorption spectra. Crystal data for (*R*)/(*S*)-**1,** and (*R*)/(*S*)-**2** were determined by X-ray diffraction analysis at 150 K using Oxford Diffraction Gemini E system with Cu$_{K\alpha}$ radiation λ = 1.5418 Å, and details of the structure refinement are given in Table S2. CCDC number: 1564392-1564395 containing the supplementary crystallographic data for this paper can be obtained free of charge from the Cambridge Crystallographic Data Centre *via* www.ccdc.cam.ac.uk/data_request/cif. Electrochemical measurements were carried out with a BAS CV-50W voltammetric analyzer. The cell comprised inlets for a glassy carbon disk working electrode, 2.0 mm in diameter, and a silver-wire counter electrode. The reference electrode was Ag/Ag+ connected to the solution by a Luggin capillary whose tip was placed close to the working electrode. Results were corrected for junction potentials by being referenced internally to the ferrocenium/ferrocene (Fc^+/Fc) couple [$E_{1/2}(Fc^+/Fc) = +0.50$ V vs. SCE]. Potentials in this paper are referenced to the SCE. Typically, a 0.1 M solution of $[NBu_4][ClO_4]$ in CH_2Cl_2 containing 0.5 mM of sample was purged with nitrogen for 10 min, then voltammograms were recorded at ambient temperature. The scan rate was 100 mV s^{-1} for CV. The magnetic measurements were performed on MPMS-3 SQUID magnetometer on polycrystalline samples.

Computational details of electrostatic potential.

The DFT method of M06-GD3BJ/6-311+G(2df,p)/SDD was used to calculate the electronic structures [**1**, **2**, and $Tb(Pc)_2$] and the electrostatic potential for all the calculations were carried out by using Gaussian 09 (Version D.01),[S5] Multiwfn (Version 3.4 dev),[S6] and VMD (Version 1.9.1) program.[S7]

The electrostatic potential can be calculated using the following equation:

$$V_{ESP}(\vec{r}) = V_{nuc}(\vec{r}) + V_{ele}(\vec{r}) = \sum_A \frac{Z_A}{|\vec{r} - \vec{R}_A|} - \int \frac{\rho(\vec{r}\,')}{|\vec{r} - \vec{r}\,'|} d\vec{r}\,'$$

where V_{ESP} is the total electrostatic potential, V_{nuc} is the electrostatic potential of all the nucleus, V_{ele} is the electrostatic potential of the whole electronic cloud, Z_A is the atomic number of each nucleus, and ρ is the electronic density.

After the optimization of a bis(phthalocyaninato) terbium double-decker compound, the electronic density can be divided into two parts, including the contributions from terbium atom (named as ρ_{Tb}) and peripheral ligands (named as ρ_L).

$$\rho(\vec{r}) = \rho_{Tb}(\vec{r}) + \rho_L(\vec{r})$$

$$\rho_{Tb}(\vec{r}) = \sum_{i \in Tb} \mu_i C_{l,i} \chi_l(\vec{r})$$

$$\rho_L(\vec{r}) = \sum_{i \notin Tb} \mu_i C_{l,i} \chi_l(\vec{r})$$

where μ_i is the occupying number of the ith orbital; χ_l is the lth basis function in the ith orbital; $C_{l,i}$ is the element of lth row, and jth column in the expansion coefficient matrix.

When ρ_{Tb} is set to zero, the electrostatic potential of ligands (V_L) can be independently considered in the following manner.

$$V_L(\vec{r}) = V_{nuc \neq Tb}(\vec{r}) + V_{ele \notin Tb}(\vec{r}) = \sum_{A \neq Tb} \frac{Z_A}{|\vec{r} - \vec{R}_A|} - \int \frac{\rho_L(\vec{r}')}{|\vec{r} - \vec{r}'|} d\vec{r}'$$

It is worth noting that the sample dots of *Gaussian* cube file are specially set for the three bis(phthalocyaninato) terbium double-decker compounds (unit: Bohr):

For Tb{Pc(OBNP)$_4$}$_2$:

369	–4.000647	–4.004115	–3.933724
40	0.205128	0.000000	0.000000
40	0.000000	0.205128	0.000000
40	0.000000	0.000000	0.205128

For Tb(Pc){Pc(OBNP)$_4$}:

241	–4.000647	–4.004115	–3.933724
40	0.205128	0.000000	0.000000
40	0.000000	0.205128	0.000000
40	0.000000	0.000000	0.205128

For Tb(Pc)$_2$:

112	–4.000647	–4.004115	–3.933724
40	0.205128	0.000000	0.000000
40	0.000000	0.205128	0.000000
40	0.000000	0.000000	0.205128

The above cubes are defined at the *Output File Formats* in the explanation of the *cubegen* keyword. (*Gaussian 09 User's Reference*, Manual Version 8.5, Page 309)

In addition, the electrostatic potential of ligands is drawn on a 2.015 Å radius sphere centered at the Tb^{3+} position caused by the ligands. When the potential projection is drawn in VMD (Version 1.9.1), the detailed setting code is as following:

```
mol new L.cube
mol addfile sphere.cube
mol delrep 0 top
mol representation CPK 0.3 0.3 50.0 50.0
mol addrep top
mol representation Isosurface 0.0001 1 0 0 1 1
mol color Volume 0
mol addrep top
mol scaleminmax top 1 -2.0 1.0
color scale method BGR
color Display Background white
```

where *L.cube* is the cube file of V_L, while *sphere.cube* is an electronic density cube file in which only one hydrogen atom locates at the Tb^{3+} position. The sole usage of *sphere.cube* is the generation of a sphere centered in the Tb^{3+} position.

Preparation of (*R*)- and (*S*)-Tb[Pc(OBNP)$_4$]$_2$ (1). A mixture of (*R*)-/(*S*)-benzo[*b*]dinaphtho[2,1-*e*:1',2'-*g*][1,4]dioxocine-5,6-dicar-bonitrile (200 mg, 0.49 mmol), $Tb(acac)_3 \cdot nH_2O$ (32 mg, 0.08 mmol), and DBU (0.05 ml) in *n*-pentanol (4 mL) was heated to reflux under nitrogen for 8 h. After being cooled to room temperature, the volatiles were removed under reduced pressure and the residue was purified by chromatography on a silica-gel column using $CHCl_3$/*n*-hexane (2:1) as eluent. The crude product was purified by repeated chromatography followed by recrystallization from $CHCl_3$ and methanol, giving the pure target compound as a dark green powder in the yield of 68 mg (32%). MS (MALDI-TOF): calcd for $C_{224}H_{112}N_{16}O_{16}Tb$ $(M)^+$ 3441.8; an isotopic cluster peaking at m/z 3442.1. Anal. Calcd (%) for (*R*)-$C_{224}H_{112}N_{16}O_{16}Tb \cdot 5CHCl_3 \cdot 3H_2O$: C, 67.20; H, 3.02; N, 5.48;

found: C, 67.05; H, 3.12; N, 5.48. Anal. Calcd (%) for (*S*)-$C_{224}H_{112}N_{16}O_{16}Tb \cdot 6CHCl_3 \cdot 3H_2O$: C, 65.58; H, 2.97; N, 5.32; found: C, 65.79 ; H, 3.00 ; N, 5.39.

Preparation of (*R*)- and (*S*)-Tb(Pc)[Pc(OBNP)$_4$] (2). A mixture of (*R*)-/(*S*)-benzo[*b*]dinaphtho[2,1-*e*:1',2'-*g*][1,4]dioxocine-5,6-dicarbonitrile (100 mg, 0.24 mmol), Tb(Pc)(acac) (42 mg, 0.06 mmol), and DBU (0.05 ml) in *n*-pentanol (3 mL) was heated to reflux under nitrogen for 6 h. After being cooled to room temperature, the volatiles were removed under reduced pressure and the residue was purified by chromatography on a silica-gel column using CH_2Cl_2/*n*-hexane (3:1) as eluent. The crude product was purified by repeated chromatography followed by recrystallization from CH_2Cl_2 and methanol, giving the pure target compound as a green powder in the yield of 29 mg (22%). MS (MALDI-TOF): calcd for $C_{144}H_{72}N_{16}O_8Tb$ $(M+H)^+$ 2313.5; an isotopic cluster peaking at m/z 2313.4. Anal. Calcd (%) for (*R*)-$C_{144}H_{72}N_{16}O_8Tb \cdot C_6H_{14} \cdot 1.5CH_2Cl_2$: C, 72.02; H, 3.55; N, 8.87; found: C, 72.42; H, 3.48; N, 8.85. Anal. Calcd (%) for (*S*)-$C_{144}H_{72}N_{16}O_8Tb \cdot C_6H_{14} \cdot 0.5CH_2Cl_2$: C, 74.02; H, 3.59; N, 9.18; found: C, 75.00; H, 3.45; N, 9.16.

Spectroscopic Characterization. Satisfactory elemental analysis results were obtained for both compounds **1** and **2** after repeated column chromatography and recrystallization. These compounds have also been characterized by MALDI-TOF mass spectroscopy, with the MALDI-TOF mass spectrum exemplified by (*S*)-**2** given in Fig. S14.

The electronic absorption spectra of **1** and **2** were recorded in $CHCl_3$ and the data are summarized in Table S7. As can be seen in Fig. S1-S3, both **1** and **2** exhibit typical feature of the electronic absorption spectra for bis(phthalocyaninato) double-decker complexes with the phthalocyanine Q bands appearing at 674-678 nm with one vibrational shoulder at 606-610 nm, and the phthalocyanine Soret bands at *ca.* 360 nm. Observation of the typical π-radical anion-related bands at *ca.* 480, 912-922, and 1400-1600 nm reveals the presence of an unpaired electron in both species, which contributes to optimize the SMM properties by interacting with the f electrons of terbium.[S2, S8] The intense band observed at *ca.* 325 nm is attributed to the absorption of binaphthyl groups. The magnetic circular dichroism (MCD) spectra of **1** and **2** show significant dispersion-type Faraday A term signals with strong negative to positive peaks observed at 679/665 and 679/668 nm, respectively, in the Q-band region, Fig. S1 and S2, suggesting the transitions to the nearly degenerate excited states of these absorptions.[S9]

The circular dichroism (CD) spectra of the two chiral double-decker complexes **1** and **2** recorded in $CHCl_3$ are also shown in Fig. S1 and S2. As expected, nearly perfect mirror-image CD spectra are observed almost in the whole spectral region of the optically pure isomers of **1** and **2** with the CD intensity ranging from $[\theta] = 10^6$ to 10^7 mdeg dm^3 mol^{-1} cm^{-1}.[S9] This indicates the effective chiral information transfer from the peripheral chiral binaphthyl units to the central phthalocyanine chromophores in the double-decker molecules, which in turn results in an intensified electronic anisotropy for both species in comparison with corresponding homoleptic unsubstituted bis(phthalocyaninato) rare earth counterparts. For the (*R*)-enantiomer of the homoleptic double-decker **1**, the CD sign is positive in the whole electronic absorption region from 300 to 800 nm, while the CD sign for (*R*)-**2** is positive between 300 and 550 nm, whereas negative between 550 and 720 nm.

Dilution Magnetic Studies. For the purpose of further clarifying the intermolecular ferromagnetic coupling between adjacent double-decker molecules within the pseudo quadruple-decker supramolecular structure as well as the effect on the magnetic performance of Tb(Pc){Pc(OBNP)$_4$} (**2**), the magnetic measurement for the diamagnetic yttrium-diluted sample (*S*)-Tb$_{0.17}$Y$_{0.83}$(Pc){Pc(OBNP)$_4$} was also conducted**.** Fig. S7c shows the temperature dependence of the magnetic susceptibility $\chi_m T$ of this diluted sample. The $\chi_m T$ value for (*S*)-Tb$_{0.17}$Y$_{0.83}$(Pc){Pc(OBNP)$_4$} at 300 K is 13.58 cm^3·K·mol^{-1}, consistent with the expected value of 14.00 cm^3·K·mol^{-1} expected for one Tb(III) ion [$^7F_6$, S = 3, L = 3, g = 3/2] with six times of organic radicals (S = 1/2).[S2] Different from the undiluted sample Tb(Pc){Pc(OBNP)$_4$} (**2**), the χ_MT *vs.* T curve of the diluted sample shows a decrease tendency along with lowering the temperature without a rising tendency at low temperature, revealing the significant decrease of the intermolecular ferromagnetic coupling through diamagnetic dilution**.** The dynamic magnetic property of the diluted powder sample of **2** was also investigated under zero Oe. As displayed in Fig. S11, (*S*)-Tb$_{0.17}$Y$_{0.83}$(Pc){Pc(OBNP)$_4$} exhibits the temperature dependent character in both in-phase signal (χ') and out-of-phase signal (χ'') with an energy barrier of U_{eff} = 806 (10) K and τ_0 = 5.7×10^{-12} s. These values are comparable with those found for the undiluted sample

Tb(Pc){Pc(OBNP)$_4$} (**2**), disclosing the very small effect of the intermolecular ferromagnetic coupling within the pseudo quadruple-decker supramolecular structure on the magnetic properties of the unsymmetrical double-decker SIM.

References

[S1]J. G. Stites, C. N. McCarty and L. L. Quill, *J. Am. Chem. Soc.*, 1948, **70**, 3142.

[S2]Y. Chen, F. Ma, X. Chen, B. Dong, K. Wang, S. Jiang, C. Wang, X. Chen, D. Qi, H.-L. Sun, B.-W. Wang, S. Gao and J. Jiang, *Inorg. Chem.*, 2017, **56**, 13889.

[S3](a) K. Wang, D. Qi, H. Wang, W. Cao, W. Li and J. Jiang, *Chem.–Eur. J.*, 2012, **18**, 15948. (b) H. Zhou, K. Wang, D. Qi and J. Jiang, *Dalton Trans.*, 2014, **43**, 1699.

[S4] (a) J. L. J. A. Rikken and E. Raupach, *Nature*, 1997, **390**, 493. (b) C. Train, R. Gheorghe, V. Krstic, L. Chamoreau, N. S. Ovnesyan, G. L. J. A. Rikken, M. Gruselle and M. Verdaguer, *Nat. Mater.*, 2008, **7**, 729. (c) Y. Kitagawa, H. Segawa and K. Ishii, *Angew. Chem.*, 2011, **123**, 9299. (d) Y. Kitagawa, T. Miyatakeb and K. Ishii, *Chem. Commun.*, 2012, **48**, 5091. (e) S. Bordács, I. Kézsmárki, D. Szaller, L. Demkó, N. Kida, H. Murakawa and Y. Onose, *Nat. Phys.*, 2012, **8**, 734. (f) K. Wang, S. Zeng, H. Wang, J. Dou and J. Jiang, *Inorg. Chem. Front.*, 2014, **1**, 167.

[S5]M. J. Frisch, G. W. Trucks, H. B. Schlegel, G. E. Scuseria, M. A. Robb, J. R. Cheeseman, G. Scalmani, V. Barone, B. Mennucci, G. A. Petersson, H. Nakatsuji, M. Caricato, X. Li, H. P. Hratchian, A. F. Izmaylov, J. Bloino, G. Zheng, J. L. Sonnenberg, M. Hada, M. Ehara, K. Toyota, R. Fukuda, J. Hasegawa, M. Ishida, T. Nakajima, Y. Honda, O. Kitao, H. Nakai, T. Vreven, J. A. Montgomery, Jr., J. E. Peralta, F. Ogliaro, M. Bearpark, J. J. Heyd, E. Brothers, K. N. Kudin, V. N.

Staroverov, T. Keith, R. Kobayashi, J. Normand, K. Raghavachari, A. Rendell, J. C. Burant, S. S. Iyengar, J. Tomasi, M. Cossi, N. Rega, J. M. Millam, M. Klene, J. E. Knox, J. B. Cross, V. Bakken, C. Adamo, J. Jaramillo, R. Gomperts, R. E. Stratmann, O. Yazyev, A. J. Austin, R. Cammi, C. Pomelli, J. W. Ochterski, R. L. Martin, K. Morokuma, V. G. Zakrzewski, G. A. Voth, P. Salvador, J. J. Dannenberg, S. Dapprich, A. D. Daniels, O. Farkas, J. B. Foresman, J. V. Ortiz, J. Cioslowski, and D. J. Fox, *Gaussian 09, Version D.01*, Gaussian, Inc., Wallingford CT, **2013**.

[S6] T. Lu and F. Chen, *J. Comp. Chem.*, 2012, **33**, 580.

[S7] W. Humphrey, A. Dalke and K. Schulten, *J. Molec. Graphics*, 1996, **14**, 33.

[S8]H. Wang, B. Wang, Y. Bian, S. Gao and J. Jiang, *Coord. Chem. Rev.*, 2016, **306**, 195.

[S9](a) W. Lv, P. Zhu, Y. Bian, C. Ma, X. Zhang and J. Jiang, *Inorg. Chem.*, 2010, **49**, 6628. (b) Y. Zhou, Y. Zhang, H. Wang, J. Jiang, Y. Bian, A. Muranaka and N. Kobayashi, *Inorg. Chem.*, 2009, **48**, 8925. (c) X. Zhang, A. Muranaka, W. Lv, Y. Zhang, Y. Bian, J. Jiang and N. Kobayashi, *Chem.–Eur. J.*, 2008, **14**, 4667.

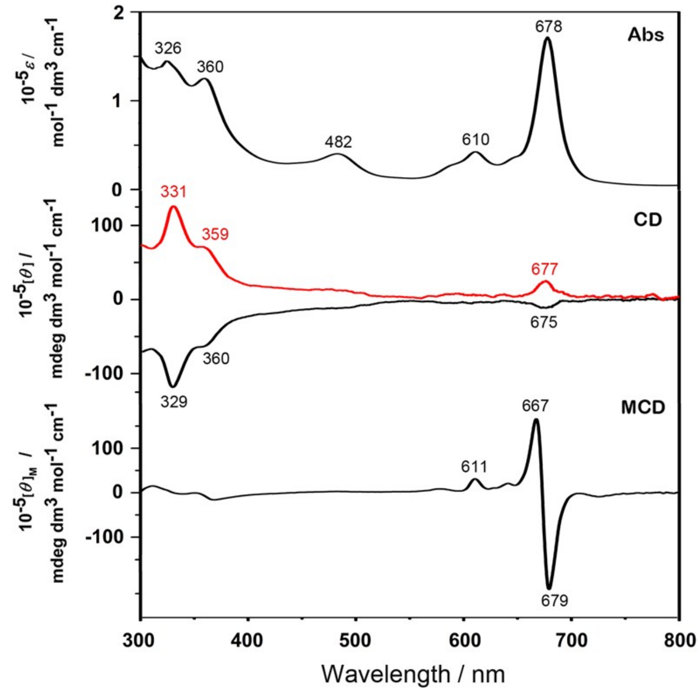

Fig. S1. Electronic absorption, CD, and MCD spectra of **1** in $CHCl_3$. Black and red lines are used to plot the CD spectra of the (*S*)- and (*R*)-enantiomers, respectively.

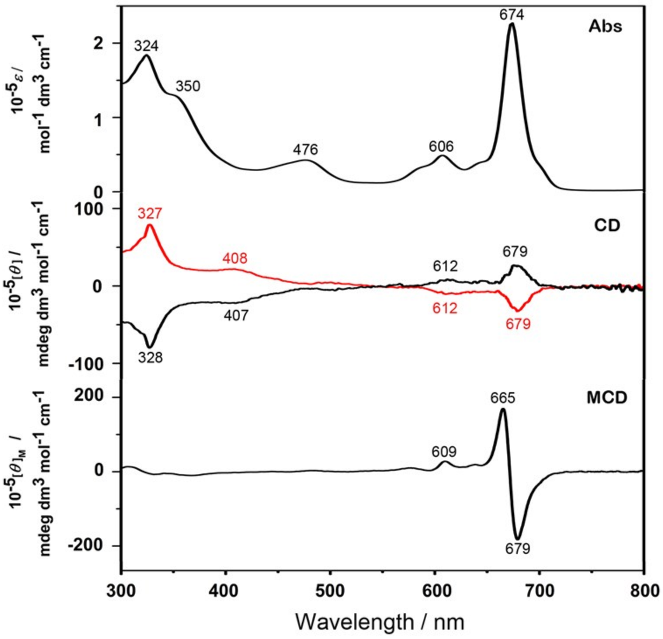

Fig. S2. Electronic absorption, CD, and MCD spectra of **2** in $CHCl_3$. Black and red lines are used to plot the CD spectra of the (*S*)- and (*R*)-enantiomers, respectively.

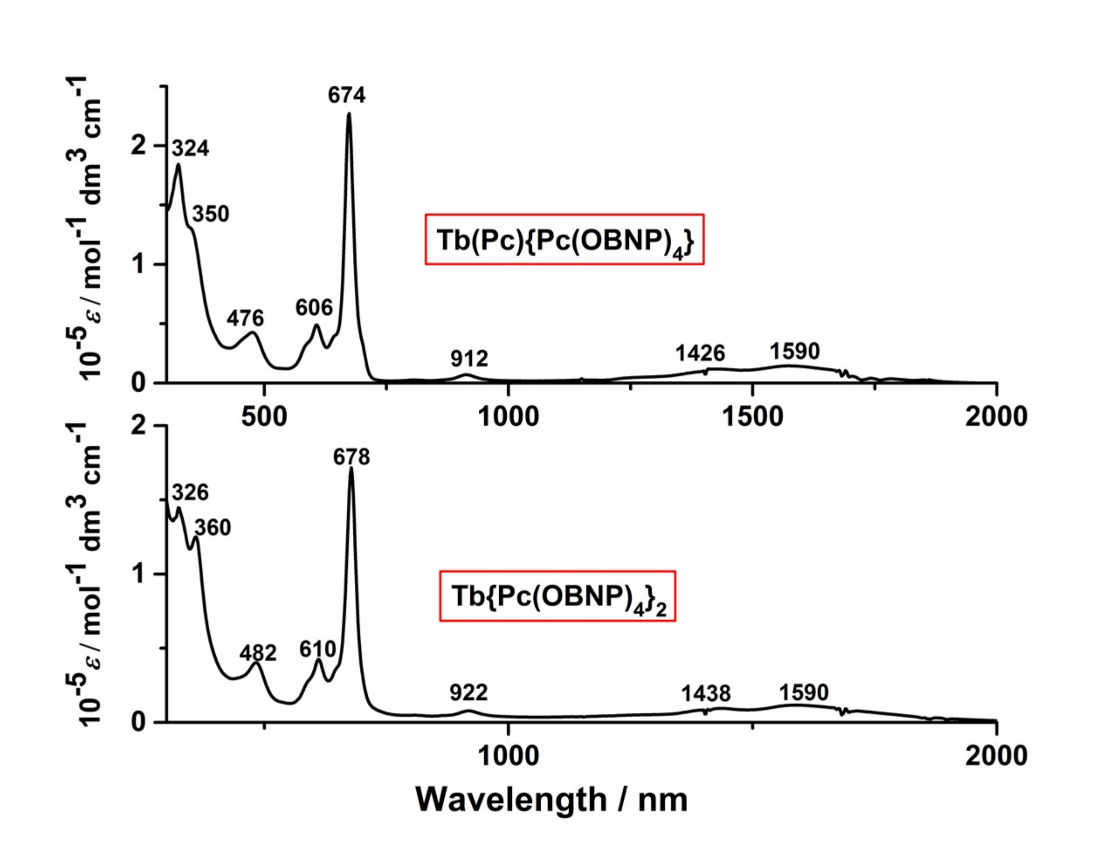

Fig. S3. Electronic absorption spectra of **1** and **2** in $CHCl_3$.

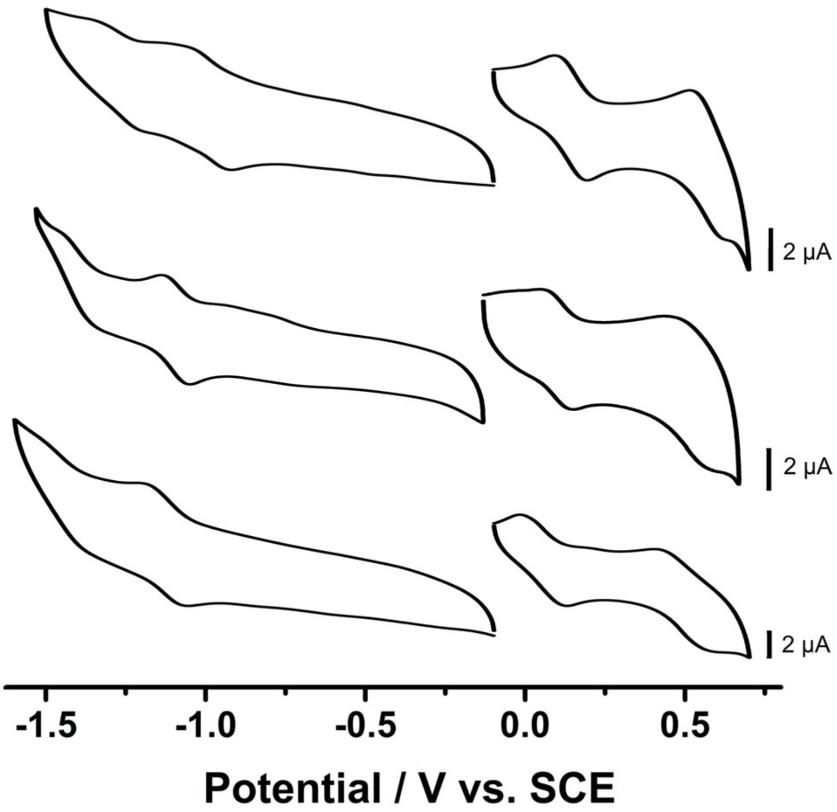

Fig. S4. Cyclic voltammogram of **1** (top), **2** (middle), and Tb(Pc)$_2$ (bottom) in CH_2Cl_2 containing 0.1 mol dm^{-3} [Bu_4N][ClO_4] at a scan rate of 100 mV s^{-1}.

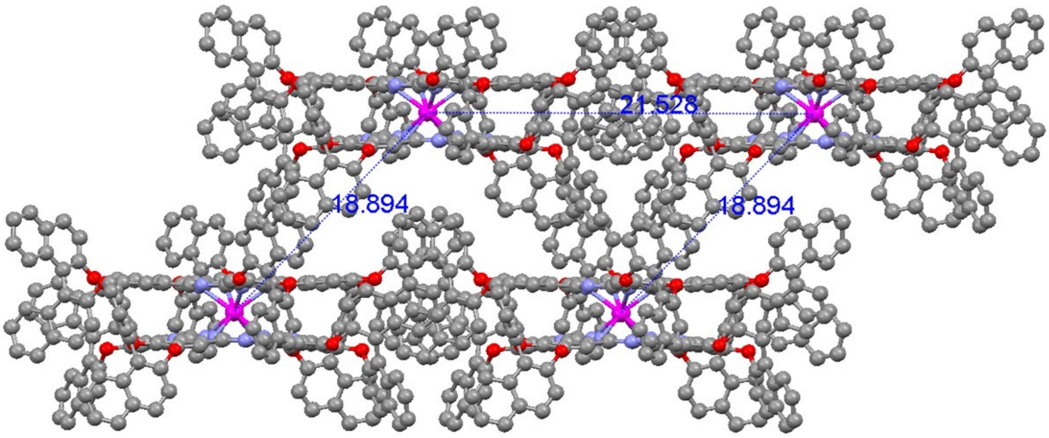

Fig. S5. Molecular packing in single crystals of (*S*)-**1** with hydrogen atoms omitted for clarity [Tb(III) pink, C gray, N blue, O red].

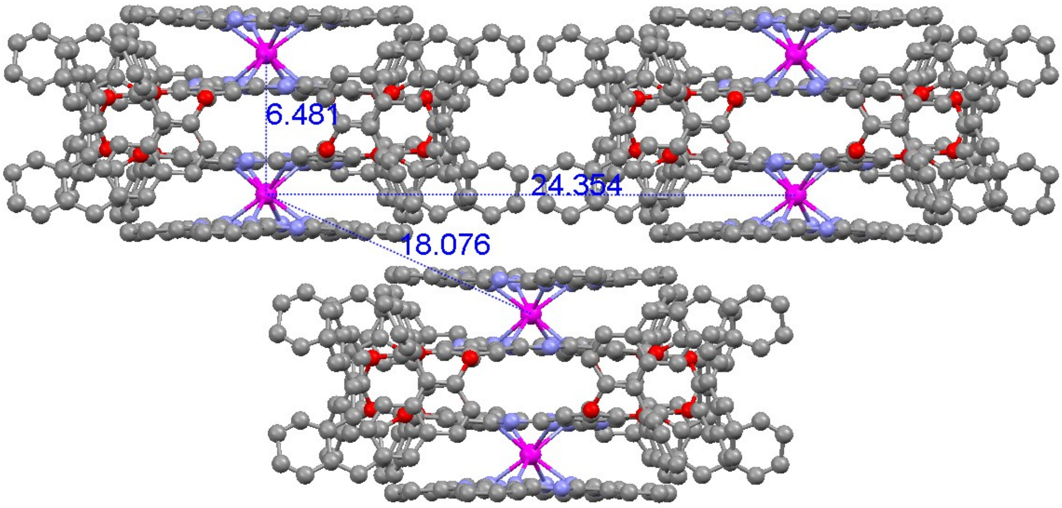

Fig. S6. Molecular packing in single crystals of (*S*)-**2** with hydrogen atoms omitted for clarity [Tb(III) pink, C gray, N blue, O red].

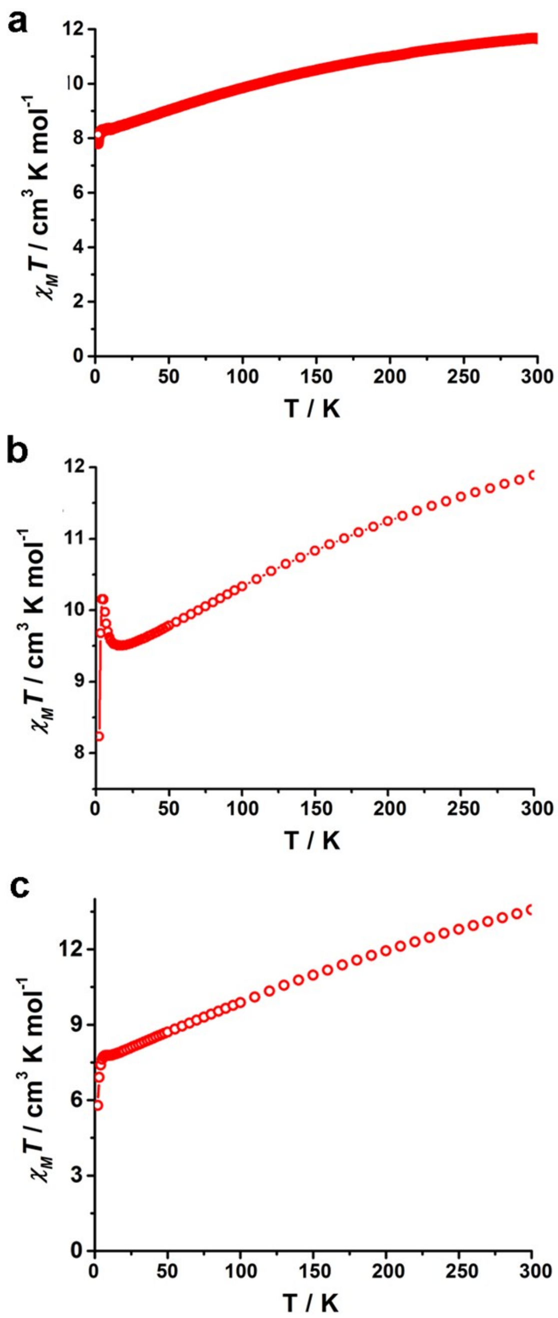

Fig. S7. Temperature dependence of $\chi_M T$ for **1** (a), **2** (b), and the diamagnetic yttrium-diluted sample (*S*)-$Tb_{0.17}Y_{0.83}$(Pc){Pc(OBNP)$_4$} (c).

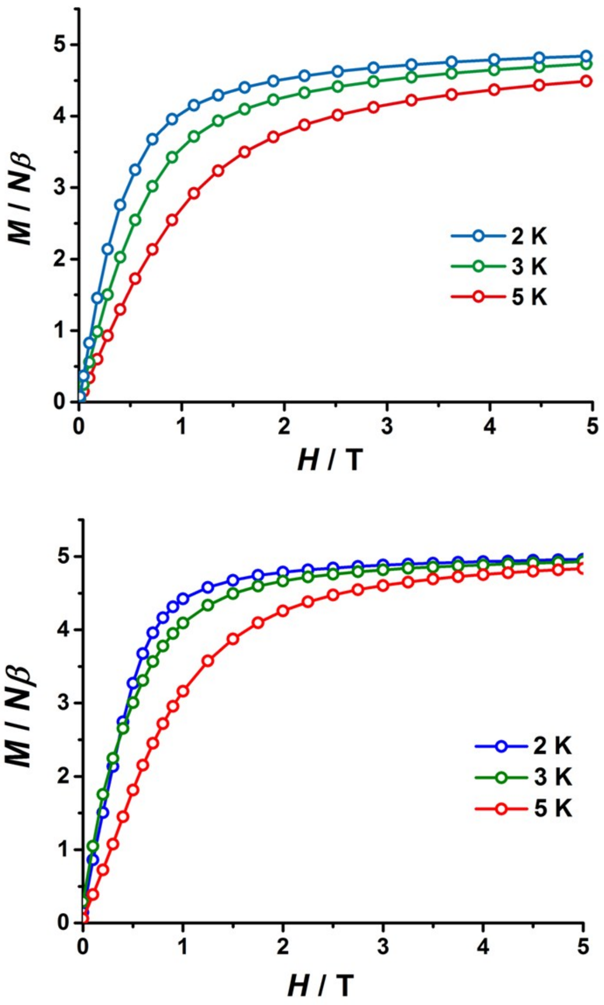

Fig. S8. The *M vs H* curves for **1** (top) and **2** (bottpm) at 2, 3, and 5 K.

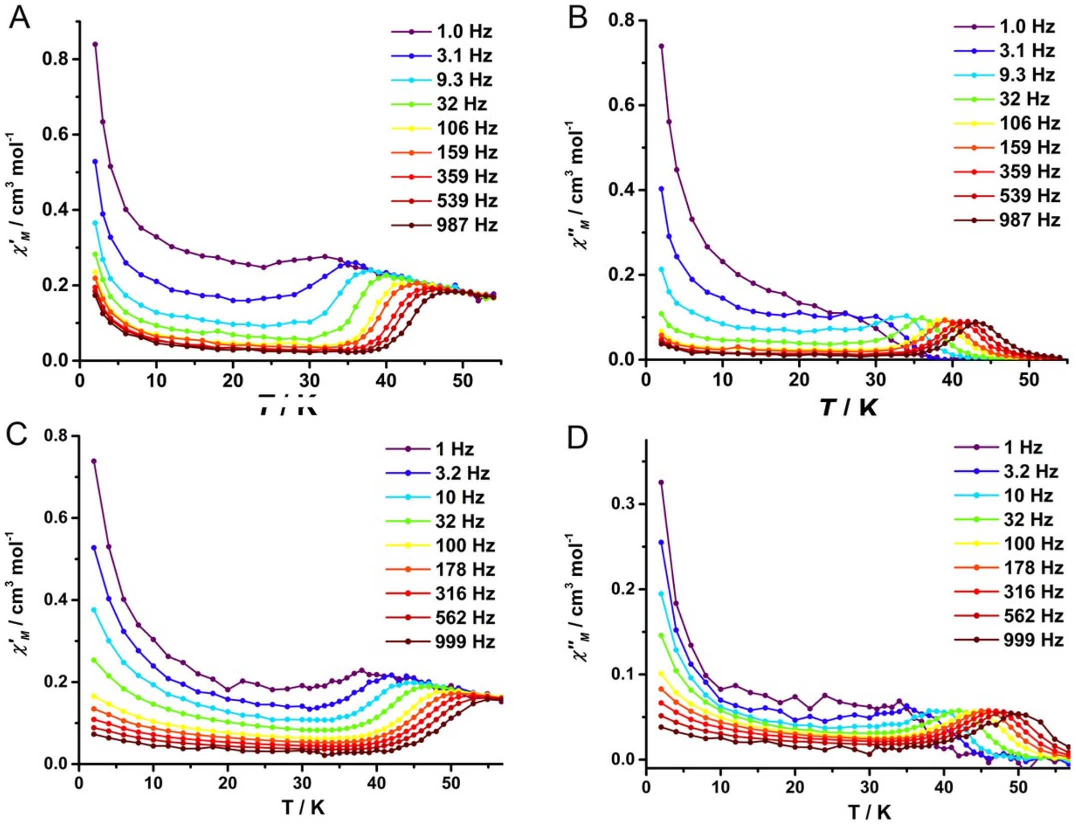

Fig. S9. Temperature dependence of the in-phase (χ') and out-of-phase (χ'') ac magnetic susceptibility of **1** [(A) for χ', (B) for χ''] and **2** [(C) for χ', (D) for χ''] under zero applied dc field.

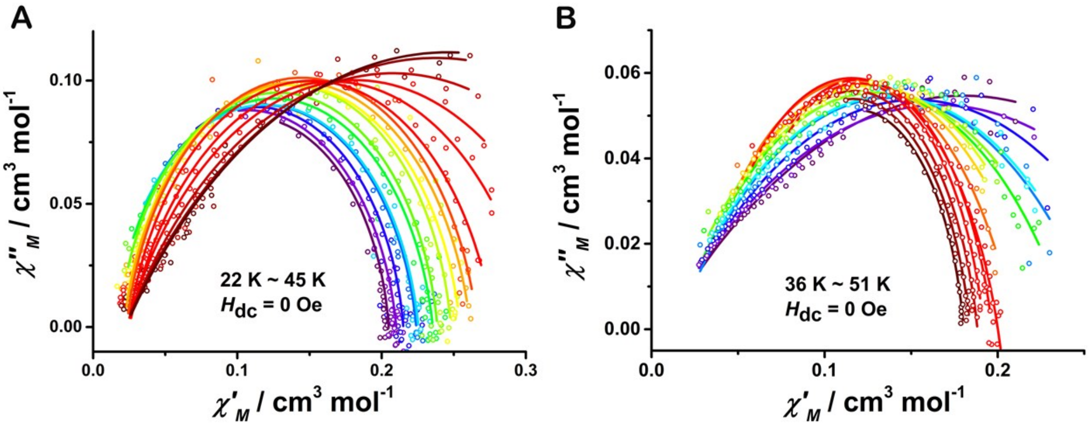

Fig. S10. Cole-Cole diagrams of **1** (A) and **2** (B) with the ac susceptibility data at 24−45 K and 36−51 K, respectively, under a zero applied dc field. The solid lines are the best fit to Debye's law.

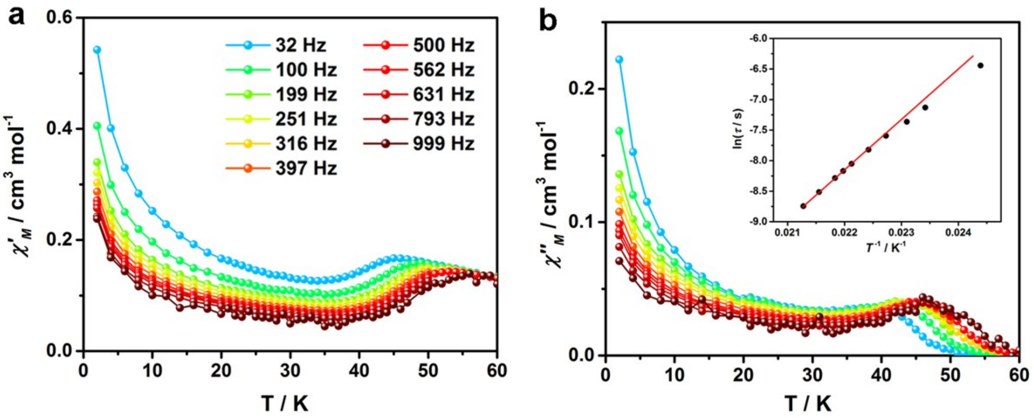

Fig. S11. Temperature dependence of χ' (a) and χ'' (b) ac magnetic susceptibility of the diamagnetic yttrium-diluted sample (*S*)-$Tb_{0.17}Y_{0.83}(Pc)\{Pc(OBNP)_4\}$ under zero applied dc field. Inside: the plots of ln(*τ*) *vs*. 1/*T* for the diamagnetic yttrium-diluted sample (*S*)-$Tb_{0.17}Y_{0.83}(Pc)\{Pc(OBNP)_4\}$ under zero dc field.

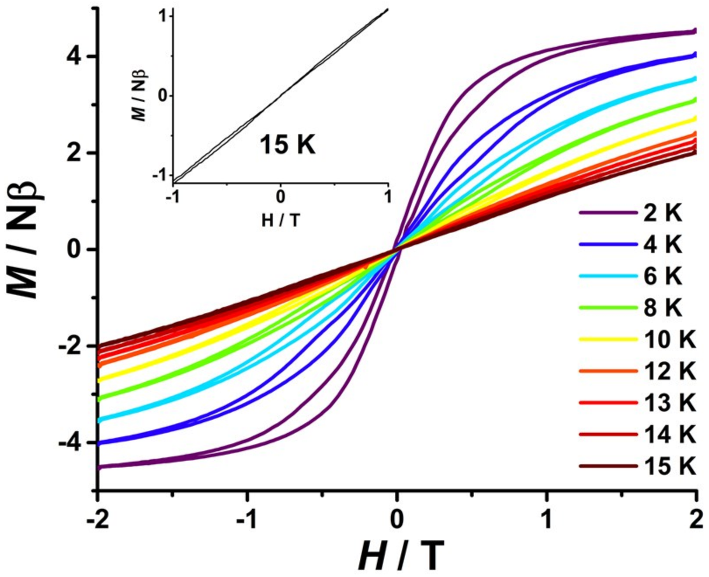

Fig. S12. Normalized magnetic hysteresis loops of **1** at 2−15 K under 500 Oe•s^{-1} of the magnetic field.

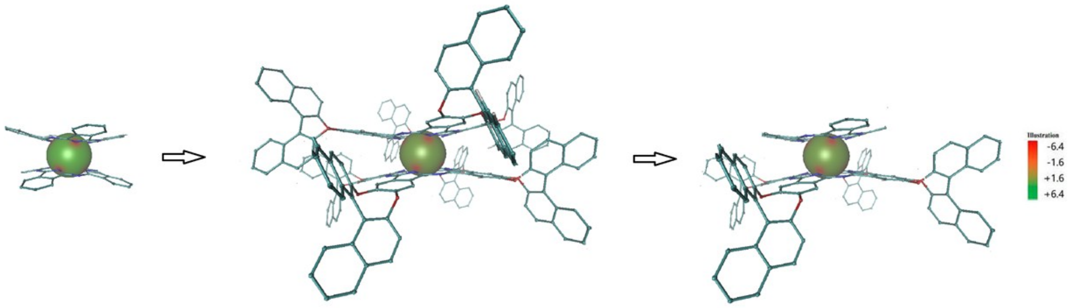

Fig. S13. Electrostatic potential around the Tb^{3+} (2 Å radius sphere) caused by the two Pc ligands.

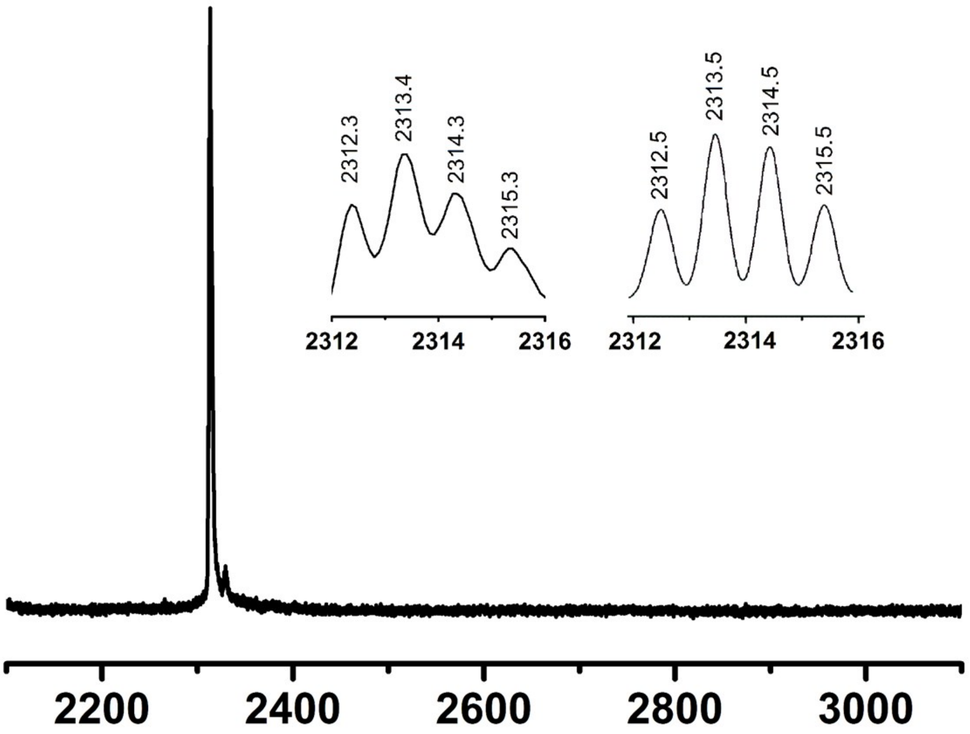

Fig. S14. The MALDI-TOF mass spectra of (*S*)-**2** as representative. Inset: Experimental (left) and simulated isotopic (right) pattern for the molecular ion of (*S*)-**2**.

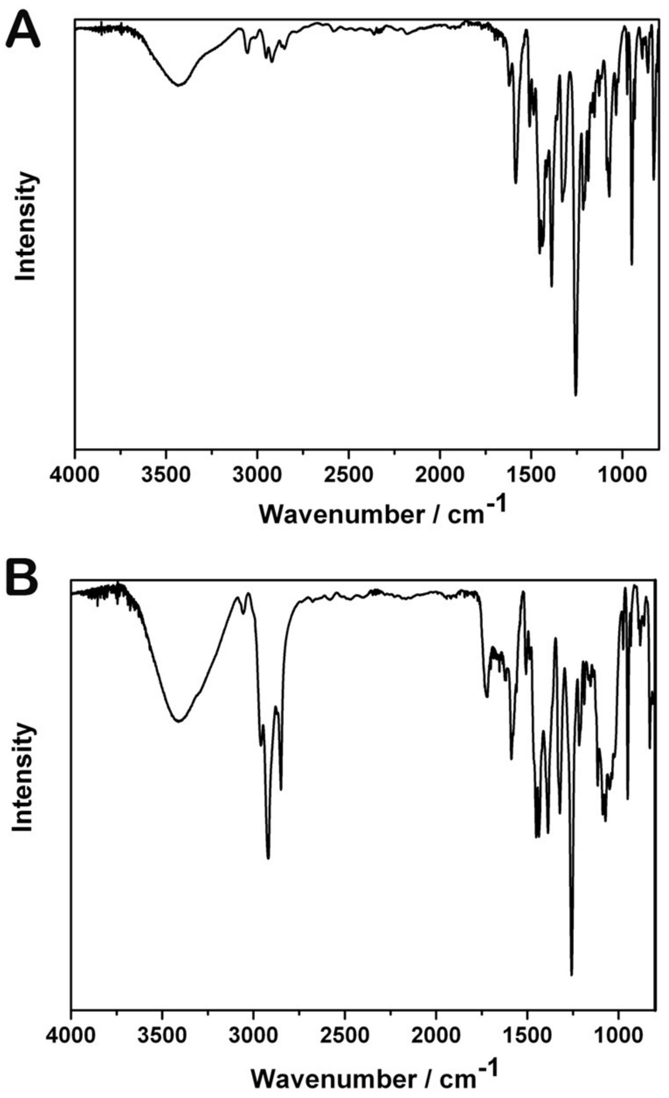

Fig. S15. IR spectra of **1** (A) and **2** (B).

Table S1. Half-wave redox potentials *vs.* SCE of **1** and **2** as well as Tb(Pc)$_2$ recorded in CH_2Cl_2 containing 0.1 mol dm^{-3} [Bu_4N][ClO_4] at a scan rate of 100 mV s^{-1}.

compound	Oxd$_1$[V]	Red$_1$[V]	Red$_2$[V]
1	0.57	0.14	-1.02
2	0.55	0.11	-1.07
Tb(Pc)$_2$	0.50	0.07	-1.13

Table S2. Crystal data and structure refinements for **1** and **2**.

Compound	**(S)-1**	**(R)-1**	**(S)-2**	**(R)-2**
formula	$C_{228}H_{120}C_{l8}N_{16}O_{16}Tb$	$C_{224}H_{112}N_{16}O_{16}Tb$	$C_{144}H_{72}N_{16}O_{8}Tb$	$C_{144}H_{72}N_{16}O_{8}Tb$
fw	3781.91	3442.21	2313.11	2313.11
crystal system	Tetragonal	Tetragonal	Tetragonal	Tetragonal
space group	I_4	I_4	I_{422}	I_{422}
a	21.5284(5)	21.5284(5)	24.354(3)	24.4311(9)
b	21.5284(5)	21.5284(5)	24.354(3)	24.4311(9)
c	22.3817(14)	22.3817(14)	23.9482(14)	23.9514(9)
α	90	90	90	90
β	90	90	90	90
γ	90	90	90	90
V	10373.3(8)	10373.3(8)	14204(4)	14296.1(12)
Z	2	2	4	4
θ range (deg)	3.95-66.71	2.91-67.87	3.63-67.70	3.69-67.25
F_{calcd} (g/cm^3)	1.211	1.102	1.082	1.075
μ(mm^{-1})	3.139	2.170	2.898	2.879
F(000)	3858	3522	4707	4707
R_1 (I>2θ)	0.0826	0.1319	0.1092	0.1157
R_{w2} (I>2θ)	0.2208	0.2762	0.2244	0.2886
R_{w2} for all	0.2305	0.3364	0.2838	0.3347
GOF on F^2	1.059	0.757	0.838	1.030
CCDC number	1564394	1564392	1564395	1564393

Table S3. Structural data for the double-deckers **1** and **2** as well as $TbPc_2$.

	(S)-1	**(R)-1**[a]	**(S)-2**	**(R)-2**
Average Tb-N {Pc(OBNP)$_4$} bond distance [Å]	2.425	2.353	2.428	2.424
Average Tb-N (Pc) bond distance [Å]	-----	-----	2.436	2.437
Average Tb-N_4 {Pc[Pc(OBNP)$_4$} plane distance [Å]	1.411	1.371	1.442	1.411
Average Tb-N_4 (Pc) plane distance [Å]	------	-----	1.384	1.418
Interplanar distance [Å]	2.822	2.742	2.826	2.829
Dihedral angle between the two N4 planes [°]	0	0	0	0
Average twist angle [°]	43.07	44.84	39.44	39.10
The nearest Tb…Tb distance [Å]	18.894	18.894	6.481	6.482

[a] The quality of the crystals for **(*R*)-1** was not good enough as for **(*S*)-1**. Therefore, the difference of the corresponding structural data between **(*R*)-1** and **(*S*)-1** is more significant than that for **(*R*)-2** and **(*S*)-2**.

Table S4. Relaxation fitting parameters for **1** from Least-Squares Fitting data of χ(*f*) between 1-999 Hz under zero dc field.

T / K	χ_S	χ_T	τ / s	α
24	0.0183	0.516	0.195	0.455
26	0.0175	0.496	0.165	0.452
28	0.019	0.422	0.0974	0.406
30	0.0185	0.358	0.0488	0.341
32	0.0181	0.333	0.0304	0.317
34	0.0189	0.283	0.0115	0.212
35	0.0182	0.278	0.00784	0.184
36	0.017	0.263	0.00472	0.165
37	0.0149	0.259	0.00298	0.17
38	0.0156	0.255	0.00193	0.159
39	0.0138	0.242	0.00114	0.125
40	0.0122	0.233	7.06E-04	0.122
42	0.00878	0.222	2.79E-04	0.113
44	0.0088	0.208	1.18E-04	0.0833
45	0.00955	0.202	7.92E-05	0.0663

Table S5. Relaxation fitting parameters for **2** from Least-Squares Fitting data of χ(*f*) between 1- 999 Hz under zero dc field.

T / K	χ_S	χ_T	τ / s	α
36	0.00623	0.355	0.0831	0.613
37	0.00574	0.326	0.0453	0.597
38	0.0105	0.294	0.0229	0.54
39	0.0141	0.26	0.0109	0.472
40	0.0123	0.263	0.00841	0.477
41	0.0145	0.243	0.00475	0.425
42	0.00991	0.25	0.00357	0.449
43	0.0173	0.234	0.0023	0.383
44	0.0195	0.225	0.00147	0.354
45	0.0244	0.21	9.30E-04	0.287
46	0.0311	0.2	6.33E-04	0.226
47	0.0425	0.197	5.06E-04	0.175
48	0.0463	0.192	3.63E-04	0.148
49	0.0459	0.188	2.49E-04	0.154
50	0.049	0.184	1.79E-04	0.142
51	0.0572	0.18	1.41E-04	0.115

Table S6. The electrostatic potential around the Tb^{3+} (2 Å radius sphere) caused by the two Pc ligands in Tb{$Pc(OBNP)_4$}$_2$ (**1**), Tb(Pc){$Pc(OBNP)_4$} (**2**), and $Tb(Pc)_2$.

	1	**2**	$Tb(Pc)_2$
$Pc(OBNP)_4$ ligand	−3.43 au	−2.50 au	——
Pc ligand	——	−5.15 au	−3.75 au

Table S7. Electronic absorption data for **1** and **2** in $CHCl_3$.

Compound	λ_{max}/nm (log ε)						
1	326 (5.16)	360 (5.10)	482 (4.61)	610 (4.63)	678 (5.24)	922 (3.88)	1590 (4.07)
2	324 (5.26)	350 (5.11)	476 (4.63)	606 (4.69)	674 (5.36)	912 (3.85)	1590 (4.16)